Nanoscale

View Online
Dynamic Article Links

Cite this: *Nanoscale*, 2011, **3**, 3170

www.rsc.org/nanoscale

PAPER

Nanoscale semiconductor–insulator–metal core/shell heterostructures: facile synthesis and light emission†

Gong Ping Li,[a] Rui Chen,[a] Dong Lai Guo,[a] Lai Mun Wong,[b] Shi Jie Wang,[b] Han Dong Sun[a] and Tom Wu*[a]

Received 5th April 2011, Accepted 28th April 2011
DOI: 10.1039/c1nr10352k

Controllably constructing hierarchical nanostructures with distinct components and designed architectures is an important theme of research in nanoscience, entailing novel but reliable approaches of bottom-up synthesis. Here, we report a facile method to reproducibly create semiconductor–insulator–metal core/shell nanostructures, which involves first coating uniform MgO shells onto metal oxide nanostructures in solution and then decorating them with Au nanoparticles. The semiconductor nanowire core can be almost any material and, herein, ZnO, SnO_2 and In_2O_3 are used as examples. We also show that linear chains of short ZnO nanorods embedded in MgO nanotubes and porous MgO nanotubes can be obtained by taking advantage of the reduced thermal stability of the ZnO core. Furthermore, after MgO shell-coating and the appropriate annealing treatment, the intensity of the ZnO near-band-edge UV emission becomes much stronger, showing a 25-fold enhancement. The intensity ratio of the UV/visible emission can be increased further by decorating the surface of the ZnO/MgO nanowires with high-density plasmonic Au nanoparticles. These heterostructured semiconductor–insulator–metal nanowires with tailored morphologies and enhanced functionalities have great potential for use as nanoscale building blocks in photonic and electronic applications.

1. Introduction

Heterostructures with distinct components of a semiconductor, insulator and metal are ubiquitous in conventional technologies, like electronics, photonics *etc*. In nanoscience, constructing such hierarchical nanoscale architectures entails new challenges as a result of compatibility issues during their synthesis. Nevertheless, making heterostructured semiconductor nanowires (NWs) by a bottom-up approach is a versatile way to create new functionalities that are complementary, or even inaccessible, to individual homogeneous NWs. This has attracted a lot of attention in recent years. Compared to the traditional modification strategies, such as doping,[1–5] heterostructures, in particular core/shell NWs, have unique advantages. For example, appropriate surface coating can passivate the surface states and help to improve the device performance.[6–11] Moreover, after removal of the core, hollow metal oxide nanotubes (NTs) may find many unique applications, such as in molecule and drug delivery.[12] Adding a component of noble metals can further harvest the plasmonic functionalities of the nanoparticles (NPs), increasing the structural and functional complexity. Thus, it is desirable to develop effective and scalable bottom-up approaches to synthesise such multi-component *quasi*-one-dimensional heterostructures.

A typical building block of such multi-component heterostructures is a semiconductor/insulator core/shell NW coupled with metal components. With regard to the semiconductor core, there has been lots of recent interest in the fabrication and characterization of zinc oxide (ZnO)-based heterostructures. As a typical wide band gap semiconductor, ZnO has a large band gap of 3.37 eV and an exciton binding energy of 60 meV at room temperature. The unique electronic and optoelectronic properties of ZnO enable its many promising applications in nanoelectronics and nanophotonics.[13–19] To construct heterostructures with ZnO, magnesium oxide (MgO) is a good candidate for an insulator, as it has a large band gap (7.7 eV) and has been used to alloy with ZnO to realize light-emitting devices with tunable wavelength.[20] Until now, several methods have been reported to fabricate ZnO/MgO core/shell heteronanostructures,[21–25] such as low-pressure MOCVD, MBE, metal vapor deposition and solution-based methods. However, these approaches either require complex synthesis setup or seldom realize a uniform shell coating. As we will later demonstrate, research down this line also enables the fabrication of porous MgO NTs with large surface-to-volume ratios, which has not yet been reported in the literature.

[a]*Division of Physics and Applied Physics, School of Physical and Mathematical Sciences, Nanyang Technological University, Singapore 637371. E-mail: tomwu@ntu.edu.sg; Fax: +65-67941325; Tel: +65-65141047*
[b]*Materials Science and Characterization Cluster, Institute of Materials Research and Engineering, Singapore, 11760, Singapore*

† Electronic supplementary information (ESI) available: Representative SEM and TEM images of 700 °C annealed ZnO/MgO core/shell NWs, a TEM image of an individual MgO nanocrystal inside the MgO NTs and SEM images of SnO_2 NP chains embedded in MgO NTs and comb-shaped MgO hollow nanostructures. See DOI: 10.1039/c1nr10352k

Herein, we delineate a facile and scalable bottom-up method to synthesize semiconductor–insulator–metal core/shell NWs composed of a ZnO NW core (we will also show examples of SnO_2 and In_2O_3), a uniform MgO shell and decorated Au metal NPs. We illustrate this approach in Fig. 1, summarizing the processing steps and the synthesis products. The uniform MgO shells with controllable thicknesses on several kinds of metal oxide nanostructures were coated using a facile aqueous chemical bath deposition method carried out at a low temperature (92 °C). The surface modification effect of the MgO shell on the physical properties of the ZnO NW was studied. A remarkable enhancement of the UV emission from the ZnO NWs was observed after coating of the MgO shell. Subsequently adding a layer of Au NPs can lead to further enhancement. Moreover, with either an appropriate annealing treatment or a low temperature wet etching procedure, porous MgO NTs were obtained. Our results suggest that this versatile approach, involving simple coating and annealing procedures, is capable of producing a myriad of interesting heterostructures with various complexities and improved functionalities, which will help to promote the applications of low-dimensional ZnO-based nanomaterials in functional nanodevices.

2. Experimental section

2.1 Preparation of NWs and nanobelts (NBs)

a) Ultralong ZnO NWs were fabricated on silicon substrates by thermally vaporizing a mixed source of ZnO powder and graphite powder under a flow of Ar mixed with 20% O_2 in a horizontal tube furnace. The growth took place at 920 °C and lasted for 30 mins. The details of this growth process have been described elsewhere.[26]

b) ZnO NBs were grown by the pyrolysis of ZnO powder at 1300 °C in a vacuum for 1 h. The details of this experimental method are almost identical to previous reports.[27] White wool-like products were formed on the sapphire substrates.

c) SnO_2 NWs were produced on Au-coated silicon substrates through the thermal evaporation of SnO_2 mixed with graphite powder under a flow of Ar mixed with 5% O_2 at 1100 °C for 1h, as described elsewhere.[28]

d) In_2O_3 NWs were synthesized by thermally vaporizing In_2O_3 mixed with graphite powder under a flow of Ar mixed with 0.05% O_2 at 950 °C for 30 mins. Si substrates coated with 3 nm Au layers were placed downstream, serving as the growth substrates. The details of this growth process can be found elsewhere.[5,29]

2.2 Preparation of MgO shell and porous MgO NTs

a) In a typical experiment of MgO shell coating, a pyrex glass bottle with a polypropylene autoclavable screw cap was filled with $MgCl_2 \cdot 6H_2O$ (200 mM) and urea (400 mM) to a volume of 80%. After the substrates with the as-synthesized ZnO, SnO_2 or In_2O_3 nanostructures were immersed face-down into the solution, the bottle was sealed and heated to 92 °C for 12 h. After growth, the substrates were rinsed with deionized water and dried in air at 80 °C for 2 h.

The chemical reactions involved in the formation of the MgO shell can be formulated as:[24]

$$CO(NH_2)_2 + 3H_2O \rightarrow CO_2 + 2NH_4^+ + 2OH^- \quad (1)$$

$$Mg^{2+} + 2OH^- \rightarrow Mg(OH)_2 \rightarrow MgO \quad (2)$$

b) To create porous MgO NTs, both dry and wet etching processes were used to remove the ZnO cores in the ZnO/MgO core/shell NWs. In the dry etching procedure, linear chains of short ZnO nanorods (NRs) embedded in MgO NT heterostructures and porous MgO NTs were obtained by post-annealing the ZnO/MgO NWs in H_2 (10% in Ar) at 650 or 750 °C for 1 h. In the wet etching process, porous MgO NTs were

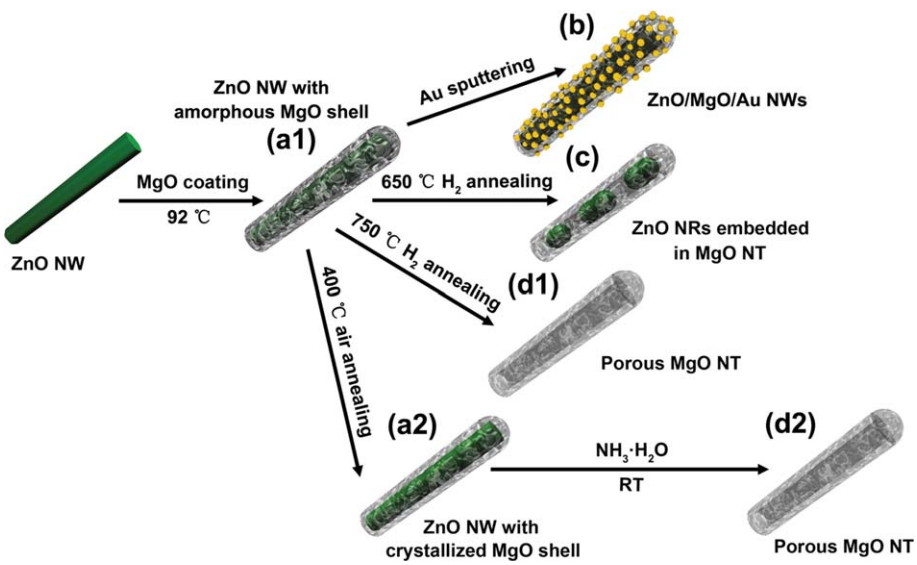

Fig. 1 A schematic illustration of the various products from our synthesis approach, including (a1 and a2) ZnO/MgO core/shell NWs, (b) ZnO/MgO core/shell NWs decorated with Au NPs, (c) linear chains of ZnO NRs embedded in MgO NTs and (d1 and d2) porous MgO NTs.

obtained by dipping the ZnO/MgO NWs in $NH_3 \cdot H_2O$ at room temperature for 24 h. To crystallize the amorphous MgO shells, the samples were post-annealed in air at relatively low temperatures (≥400 °C), before or after etching.

2.3 Characterization

The crystal structure and morphology of the samples were studied by XRD (Bruker D8 Advanced X-Ray Diffractometer), SEM (JEOL JSM-6700F), and TEM (JEOL 2100, operated at 200 kV).

Room temperature photoluminescence (PL) spectroscopy measurements were performed under excitation by a He–Cd UV laser source at 325 nm. The chemical composition was determined by X-ray photoelectron spectroscopy (XPS) (VG ESCALAB 220i-XL system equipped with a monochromatic X-ray source) in an ultra-high vacuum chamber at a pressure lower than 1.0×10^{-9} Torr. The peak positions were referenced to the adventitious C 1s peak, taken to be 285.0 eV.

3. Results and discussion

3.1 Preparation and characterization of ZnO/MgO core/shell nanostructures

Figs 2(a and b) present the scanning electron microscopy (SEM) images of the as-synthesized ZnO NWs and the heterostructured core/shell NWs. The apparent charging effect encountered during the SEM observations indicates that the shell material is much more insulating than the ZnO core. The XRD patterns of the as-grown ZnO NWs and core/shell NWs are quite similar, as shown in Fig. 2(c). Only the wurtzite ZnO phase is observed. The absence of any peak related to MgO or $Mg_xZn_{1-x}O$ implies (1) that the MgO shell is amorphous and (2) that no reaction occurs between the ZnO core and the MgO shell in this low temperature, wet chemical route. It should be mentioned here that this coating approach is universal. Since the synthesis takes place at only 92 °C, there is almost no limitation on selection of the core materials. Fig. 3 presents the SEM images of several other kinds of metal oxide nanostructures before and after the MgO shell coating. Fig. 3(a2) shows that we can also cover the MgO shell uniformly on the ZnO NBs, even on their backs and corners. Likewise, Figs 3(b2 and c2) display the homogeneous MgO shells coated on the SnO_2 and In_2O_3 NWs.

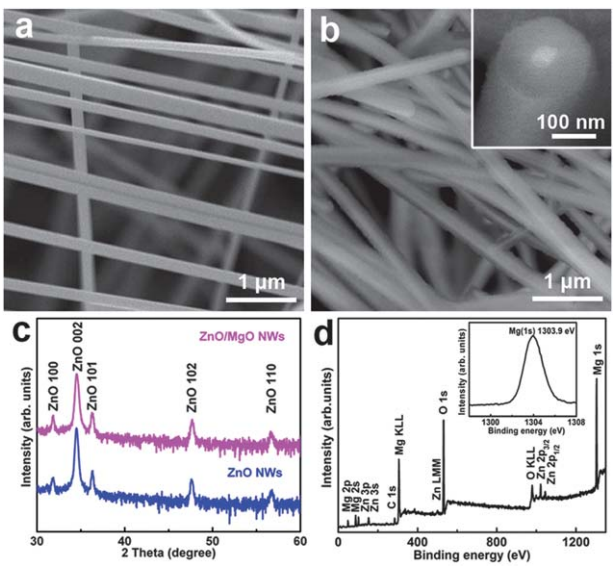

Fig. 2 SEM images of (a) uncoated ZnO NWs and (b) ZnO/MgO core/shell NWs. (c) Corresponding XRD spectra of the uncoated ZnO NWs and ZnO/MgO core/shell NWs. (d) The XPS spectrum of the as-grown ZnO/MgO core/shell NWs. The photoelectron peaks of Zn, Mg, O, C, Si were observed. The binding energy of the Mg 1s photoelectron peak was recorded at 1303.9 eV, thus confirming the presence of Mg in the form of MgO.

One salient feature of our method is its capability to give a uniform MgO coating with a tunable shell thickness. To quantitatively survey the coating uniformity, we examined multiple locations along a single core/shell NW about 35 μm in length, as shown in Fig. 3(d). The relative deviation of the shell thickness at the labeled positions is ~5%. To demonstrate the ability to control the shell thickness, we used different Mg salt concentrations with the same Mg^{2+} to urea ratio (1 : 2) to prepare the MgO shells on the ZnO NWs. As shown in Fig. 3 (e), the MgO shell thickness is almost linearly proportional to the Mg salt concentration and can be continuously tuned from 30 to 100 nm by increasing the Mg^{2+} concentration from 50 to 250 mM.

The local composition of these core/shell NWs was investigated using energy-dispersive X-ray spectroscopy (EDX) (Figs 4 (a–e)). The intensity profiles and the elemental mappings reveal a typical core/shell structure. The XPS spectrum further verified the presence of Mg in the form of MgO (Fig. 2(d)).[30] The crystallinity of the core/shell NWs was investigated using transmission electron microscopy (TEM), and the results are shown in Fig. 4(f–i). The high-resolution TEM images and selected area electron diffraction (SAED) patterns confirm that the MgO shell is amorphous. Since there is a clear core/shell boundary and the interplanar spacing in ZnO remains unchanged, the diffusion of Mg into the ZnO lattice can be ignored.

3.2 Fabrication of ZnO NRs embedded in MgO NTs and porous MgO NTs

We further fabricated some novel nanostructures based on the different thermal stability of the ZnO core and MgO shell. In a previous work, Yang *et al.* reported that a conformal Al_2O_3 covering layer could noticeably reduce the endurance of the ZnO NWs, *i.e.*, ZnO decomposes into Zn and O_2 vapors under an electron beam.[31] It is not surprising that nanoscale ZnO may decompose at much lower temperatures than the bulk counterpart, as a result of the intrinsic higher surface-to-volume ratio. Compared with Al_2O_3, MgO has a better thermal stability (melting points: MgO, 2830 °C; Al_2O_3, 2054 °C) and, thus, we expect similar behaviour. To test this hypothesis, we annealed the as-grown ZnO/MgO core/shell NWs at 700 °C in air for 12 h. The surface of the ZnO core becomes much rougher, suggesting that the defect-rich areas on the ZnO surface decompose to form voids. We did not observe this roughing effect on the uncoated ZnO NW samples under the same annealing conditions, which indicates that the MgO shell actually helps to reduce the thermal stability of the ZnO core and accelerate its decomposition (Fig. S1 in the ESI†).

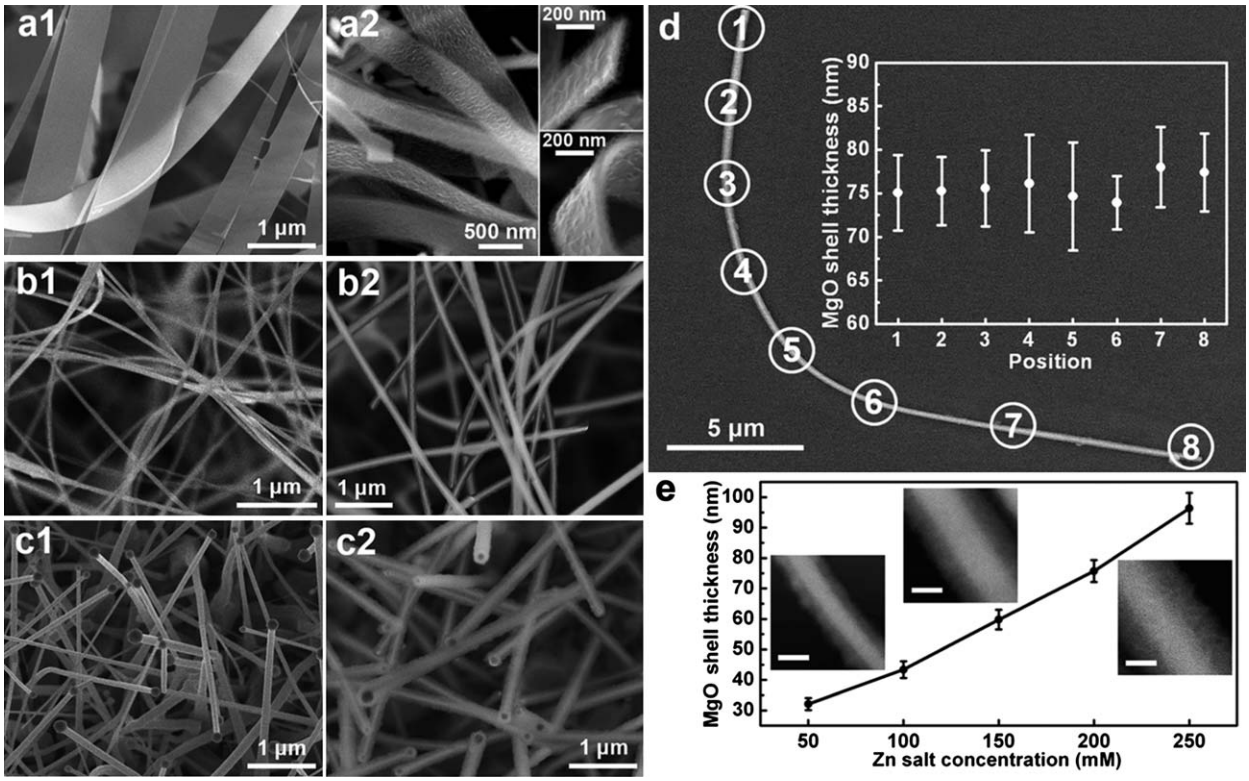

Fig. 3 SEM images of the as-grown (a1) ZnO NBs, (b1) SnO_2 NWs, (c1) In_2O_3 NWs and (a2, b2, c2) the corresponding heterostructures after MgO shell coating. The coating process took place in solution at 92 °C with $[MgCl_2] = 200$ mM and [urea] = 400 mM. (d) An SEM image of a single ZnO/MgO core/shell NW, highlighting the coating uniformity. Inset: MgO shell thickness at several selected positions. (e) The dependence of the MgO shell thickness on the $MgCl_2$ concentration. As examples, the insets show the SEM images of the ZnO/MgO core/shell NWs synthesized with $MgCl_2$ concentrations of 50, 150 and 250 mM. The scale bars in the insets represent 100 nm.

The assembly of NPs or NRs into ordered functional structures, such as chains and rings, has received lots of attention due to their unique physical properties and potential applications.[32–35] Qin *et al.* have successfully synthesized Cu NP chains encapsulated in Al_2O_3 NTs by reducing the CuO/Al_2O_3 core/shell NWs at elevated temperatures and they attributed these phenomena to the Rayleigh instability.[36] Considering that MgO has a superior thermal stability than Al_2O_3, we used a similar approach to produce linear NR chains of metals or metal oxides embedded in MgO NTs. Figs 5(a1 and a2) present the linear chains of ZnO NRs in MgO NTs obtained by reducing the ZnO/MgO core/shell NWs in H_2 (10% in Ar) at 650 °C. The ZnO NRs inside are 766.8 ± 416.7 nm in length and 153.7 ± 14.5 nm in diameter. We should note that the embedded ZnO NRs here have a cylindrical shape with large dimensions and future efforts are needed to tune their morphology and uniformity. The composition of the heterostructures was confirmed by the XRD spectrum shown in Fig. 5(a5). To our knowledge, this kind of high quality nanostructure of linear chains of ZnO NRs has not yet been reported. In a previous report,[37] an Al_2O_3 shell was coated onto the ZnO NW surface by the ALD method, but annealing of the ZnO/Al_2O_3 NWs was found to give $ZnAl_2O_4$ NTs due to the Kirkendall effect. We believe that the porous nature of the MgO shell (Fig. 5(a4)) is a critical factor in helping the Zn vapor to escape easily into the surroundings, resulting in porous MgO NTs. For other metal oxides with a higher thermal stability than ZnO, higher reducing temperatures or H_2 concentrations are needed to form similar structures. As shown in Figure S2 of the ESI†, SnO_2 NP chains embedded in MgO NT structures can be obtained by reducing the SnO_2/MgO core/shell NWs (Fig. 3(b2)) in H_2 (10% in Ar) at 1000 °C. Therefore, this general route opens up the possibility of the fabrication of many kinds of nanostructures with linear chains of metal or metal oxide NPs/NRs encapsulated in porous MgO NTs.

In order to create porous MgO NTs, both dry etching and wet etching strategies can be applied to remove the ZnO cores in the ZnO/MgO core/shell NWs. In the dry etching process, we obtained pure MgO NTs by raising the reducing temperature to 750 °C, as presented in Figs 5(a3 and a4). Similar approaches have been used to generate NTs of other materials.[38,39] According to the XRD pattern shown in Fig. 5(a5), the shell material was verified to be a spinel-like MgO phase (beta-phase, JCPDS file 30-0794).[40] The SEM images show that these MgO NTs are composed of many densely arranged nanosheets with thickness of tens of nanometres. These nanosheets are roughly vertically aligned to the NT surface. The surface area of these porous structures is much larger than the counterparts of NWs or smooth NTs, and, therefore, they may find potential applications as highly active catalysts, effective adsorbents, nanocapillaries and active material encapsulants.[23,41–43] Fig. 5(a6) shows a low-resolution TEM image of a single MgO NT and the corresponding SAED pattern. The diffraction rings correspond to the (200), (220) and (222) planes of MgO, indicating that the NTs are polycrystalline MgO, which is also consistent with the

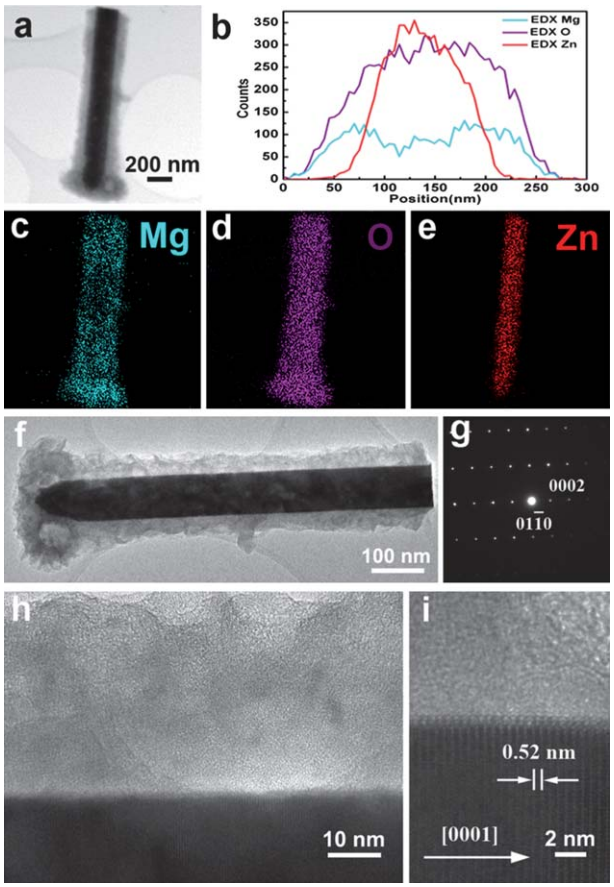

Fig. 4 (a) A TEM image of a single ZnO/MgO core/shell NW. (b) EDX line profiles of Mg, O, and Zn. (c–e) are the elemental mappings of Mg, O and Zn, respectively. (f) Typical low-resolution TEM images of an as-grown ZnO/MgO core/shell NW with a growth direction along ZnO [0001]. (g) The corresponding SAED pattern. (h) A TEM image of the ZnO/MgO interface in a core/shell NW, showing that the MgO layer is amorphous. (i) A high-resolution TEM image of the ZnO NW core.

high-resolution TEM data (inset of Figs 5(a6) and S3 of the ESI†). Comb-shaped MgO hollow nanostructures can also be achieved by post-annealing ZnO nanocomb/MgO heterostructures (Fig. S4 of the ESI†), which benefit from the conformity and homogeneity of this coating method. These results also indicate that the shape of a MgO NT is solely determined by the morphology of the ZnO core, thus offering flexibility to design nanostructures with more complexity.

Wet etching is another effective strategy to fabricate MgO NTs. The as-grown ZnO/MgO NWs were first annealed in air at 400 °C for 30 mins to crystallize the amorphous MgO shells. As shown in Fig. 5(b1), the contrast between the shell and the core becomes stronger after the annealing process. The ZnO cores were subsequently etched by $NH_3 \cdot H_2O$ at room temperature to create porous MgO NTs, which were verified by the SEM observations (Fig. 5(b2)). As shown in Fig. 5(b3), the subsequent XRD measurements confirmed that ZnO is completely absent after etching and only MgO is left behind.

We also note here that the porous MgO NTs made by both dry and wet etching possess much larger surface-to-volume ratios than the previously reported MgO NTs synthesized *via* high-temperature vapour transport growth,[23,43] which is promising for their potential applications.

3.3 Optical properties of heterostructured core/shell NWs and semiconductor–insulator–metal nanostructures

ZnO is a well-studied optical material due to its large band gap and exciton binding energy, and the synthesis strategy delineated here offers new opportunities to tailor the photoluminescence (PL) property in ZnO. For a solid state emitter based on band gap emission, it is vital to minimize any energy loss to the defects in the materials. However, for ZnO NWs, a broad defect-related radiation is often present in PL due to the large surface-to-volume ratio and the strong surface effects. Because of the energy transfer between the band edge and defect levels, controlling radiative defects, in particular near the surface, is an important issue for the improvement of emission efficiency. Here, we show that surface modification with an MgO shell is an effective method of passivating the surface states of the ZnO NW core and subsequently adjusting the PL properties. We also demonstrate that the optical properties of the core/shell NWs can be further modified by decorating their surface with Au NPs.

As presented in Fig. 6, the PL spectrum of the pure ZnO NWs consists of two bands: the near-band-edge UV emission peak at 382 nm and a broad green emission at around 520 nm. The latter emission is often related to the surface defects, in particular the oxygen vacancies.[44] Importantly, after the MgO shell coating, the intensity of the UV emission becomes much stronger than that of the uncoated ZnO sample. Similar UV enhancement effects due to covering dielectric shells have previously been reported by several other groups.[21,45–47] It was suggested that the dielectric shells with a larger band gap can passivate the non-radiative recombination centers on the core surface and reduce the separation of electron–hole pairs, thus enhancing the UV emission. Interestingly, by adjusting the heating temperature, we found that the sample annealed at 400 °C has the largest UV/defect intensity ratio, which is about 25-fold larger than that of the uncoated counterpart. As the post-annealing temperature is further increased, the intensity ratio drops. This trend cannot be explained by the annealing effect on the ZnO core alone, although air annealing usually reduces the surface oxygen vacancies.[48] To explain this PL intensity modulation, we have to consider the thermal annealing effect on the morphology evolution of the MgO nanocrystals in the shell and the formation of voids near the ZnO NW surface. At 400 °C, the MgO nanocrystals in the shell are still quite small and, thus, the attachment of the mainly amorphous shell to the ZnO core is quite effective, which gives an optimized passivation effect. As the heating temperature rises, MgO begins to crystallize and voids start to form between the ZnO core and the MgO shell, resulting in a much poorer covering of MgO and decreased UV emission. Consequently, the UV/defect ratio of the sample annealed at 700 °C is only slightly larger than that of the uncoated sample.

Considering the potential effect of strong field enhancement in noble metals due to the resonant oscillation of electrons, we decorated ZnO/MgO NWs with Au NPs. The surface plasmon (SP) resonance in metal (*e.g.*, Au, Ag and Pt) NPs is thought to modulate the PL emissions in ZnO.[10,49–52] We performed PL measurements on the vertically aligned ZnO NW samples with

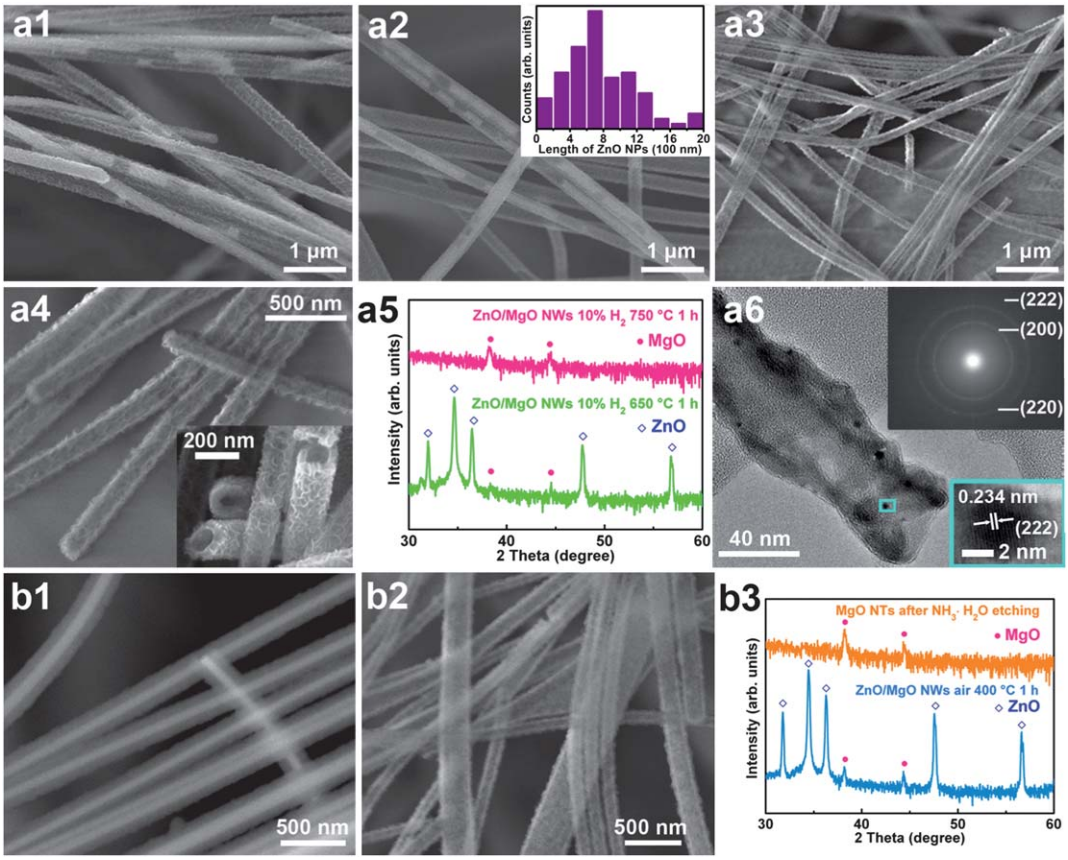

Fig. 5 An SEM image of (a1 and a2) the linear chains of ZnO NRs embedded in the MgO NTs formed by annealing ZnO/MgO NW in H_2 (10% in Ar) at 650 °C for 1 h, and (a3 and a4) the MgO NTs formed by annealing ZnO/MgO NW in H_2 (10% in Ar) at 750 °C for 1 h. The inset of (a2) presents the length distribution of the ZnO NRs in MgO NTs. (a5) XRD spectra of ZnO/MgO NWs annealed in H_2 (10% in Ar) at 650 °C and 750 °C, respectively. The ZnO NRs still maintain the wurtzite structure after annealing. (a6) A low-resolution TEM image of a single MgO NT. The insets show the corresponding SAED pattern and a high-resolution TEM image of an individual nanocrystal from the small rectangular area. An SEM image of (b1) the as-grown ZnO/MgO NWs after post-annealing in air at 400 °C and (b2) MgO NTs obtained by subsequent wet etching the sample in (b1) using $NH_3 \cdot H_2O$ for 24 h. (b3) Corresponding XRD spectra of the 400 °C post-annealed ZnO/MgO NWs and MgO NTs.

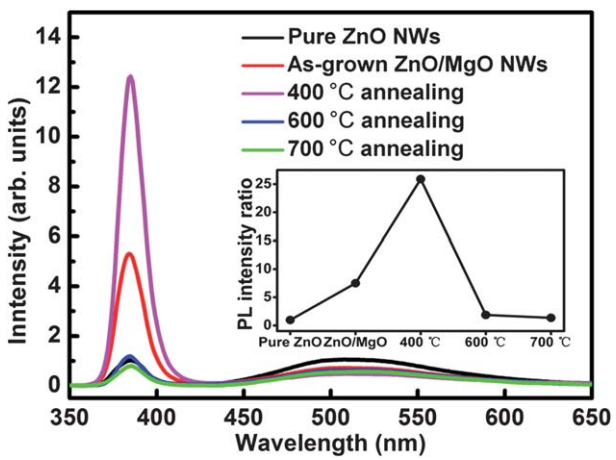

Fig. 6 Room temperature PL spectra of pure ZnO, the as-grown ZnO/MgO, and the annealed (400 °C, 600 °C and 700 °C in air) ZnO/MgO NWs. The inset presents the corresponding values of the PL intensity ratio, which is defined as the intensity ratio of the UV emission and the defect emission. All of the PL peak heights are normalized to the 382 nm peak in pure ZnO.

MgO and/or Au coating. Details of the synthesis process can be found elsewhere.[4,53] Au NPs with an average size of ~5 nm were deposited using a sputtering system (JFC-1600, JEOL). No post-annealing treatment was applied on these samples and the Au NPs were readily formed due to de-wetting between Au and MgO. Fig. 7(a) presents the SEM images of the as-synthesized ZnO/MgO core/shell NWs. The NWs remain vertically aligned after the MgO coating. We should note that the particular surface morphology of the MgO shell significantly facilitates the capture and decoration of Au NPs. During the sputtering process, the attachment would be weak as a result of the smooth surface and reflection effect if uncoated pure ZnO NWs were used. In contrast, many trapping sites exist on the rough and porous surface of the ZnO/MgO NWs, thus increasing the probability of capture of Au atoms (see the schematic diagram in Fig. 7(b)).[54,55] The corresponding SEM images confirm that there are more Au NPs covering the ZnO/MgO NWs than the pure ZnO NWs.

The PL spectra in Fig. 7(c) show that either Au or MgO coating can suppress the defect-related emission and enhance the UV emission. Interestingly, the combination of MgO and Au coating induced the largest UV enhancement, indicating that

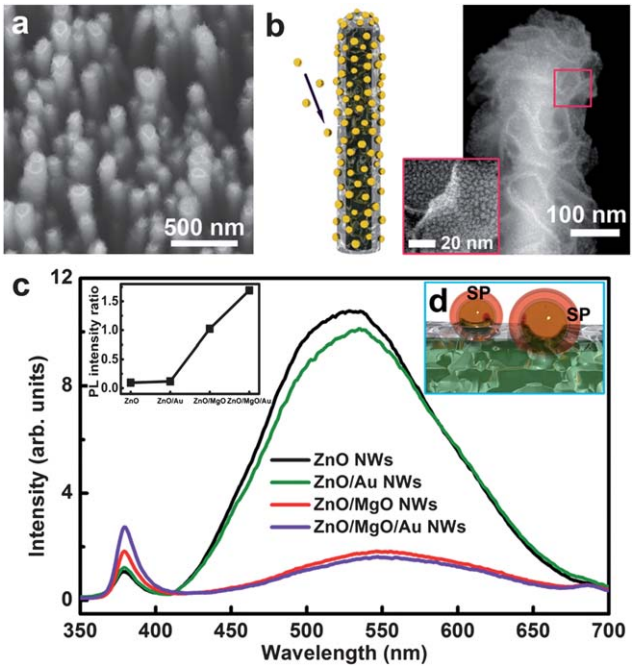

Fig. 7 SEM images of (a) the ZnO/MgO NWs and (b) ZnO/MgO/Au NWs. The inset of (b) shows a schematic illustration of sputtering Au NPs onto the ZnO/MgO NWs and the high-resolution SEM image from the pink square area. (c) Room temperature PL spectra of pure ZnO, ZnO/Au, ZnO/MgO and the ZnO/MgO/Au NWs. The left inset presents the corresponding PL intensity ratios. The right inset (d) is a schematic diagram, illustrating the interface coupling between the Au surface plasmon (SP) and ZnO NWs.

these two processes are complementary to each other. The quenching of visible light emission could be related to the strong absorption of Au NPs at these wavelengths. In the case of the ZnO/MgO/Au NWs, the insulating MgO spacer inhibits the charge transfer between ZnO and Au, thus the mechanism for UV enhancement related to electron transfer is not applicable.[49,50] Another proposed physical process for UV enhancement is the increments in the spontaneous emission rate in ZnO by the coupling of the Au SPs with the excited states in ZnO.[51,52] According to the previous calculations, the penetration depth of the Au SP fringing field into ZnO is ~70 nm.[56] After adding the spacer of the MgO shell, the coupling between the Au NPs and the ZnO core may be reduced as the spacer thickens.[57,58] On the other hand, a denser coverage of Au NPs on the ZnO/MgO/Au NWs can excite more local SPs, thus leading to a stronger enhancement of the UV emission (Fig. 7(d)). The detailed mechanism entails an in-depth understanding of the dispersion relationship of SPs within the core/shell nanostructures, as well as their dependence on the Au NP density and the interface roughness, which apparently warrants further investigation.

4. Conclusions

An MgO shell with uniform thickness was successfully coated onto several kinds of metal oxide nanostructures using a low temperature chemical bath deposition approach. The surface modification effect of the MgO covering on the thermal stability and optical properties of the ZnO NWs was investigated. Through post-annealing or low temperature wet etching, we have obtained exotic nanostructures of linear chains of short ZnO NRs encapsulated in MgO NTs and porous MgO NTs for the first time. PL measurements revealed that the UV/defect emission ratio from the ZnO NWs can be enhanced 25-fold with the MgO coating and the appropriate annealing treatment, while adding another layer of Au NPs onto the as-grown ZnO/MgO NWs can result in a 17-fold UV enhancement, without post-annealing. Our studies suggest that such heterostructured NWs derived from this facile and scalable synthesis route are promising for potential applications in photonic and electronic devices.

Acknowledgements

This work was supported by the Singapore National Research Foundation (RCA-08/018) and the Institute of Materials Research and Engineering.

References

1 X. F. Duan, Y. Huang, Y. Cui, J. F. Wang and C. M. Lieber, *Nature*, 2001, **409**, 66.
2 H. He, C. S. Lao, L. J. Chen, D. Davidovic and Z. L. Wang, *J. Am. Chem. Soc.*, 2005, **127**, 16376.
3 B. D. Yuhas, D. O. Zitoun, P. J. Pauzauskie, R. R. He and P. D. Yang, *Angew. Chem. Int. Ed.*, 2006, **45**, 420.
4 G. Z. Xing, J. B. Yi, J. G. Tao, T. Liu, L. M. Wong, Z. Zhang, G. P. Li, S. J. Wang, J. Ding, T. C. Sum, C. H. A. Huan and T. Wu, *Adv. Mater.*, 2008, **20**, 3521.
5 G. Z. Xing, J. B. Yi, D. D. Wang, L. Liao, T. Yu, Z. X. Shen, C. H. A. Huan, T. C. Sum, J. Ding and T. Wu, *Phys. Rev. B*, 2009, **79**, 174406.
6 X. G. Peng, M. C. Schlamp, A. V. Kadavanich and A. P. Alivisatos, *J. Am. Chem. Soc.*, 1997, **119**, 7019.
7 L. J. Lauhon, M. S. Gudiksen, C. L. Wang and C. M. Lieber, *Nature*, 2002, **420**, 57.
8 M. Grzelczak, M. A. Correa-Duarte, V. Salgueirino-Maceira, B. Rodriguez-Gonzalez, J. Rivas and L. M. Liz-Marztan, *Angew. Chem. Int. Ed.*, 2007, **46**, 7026.
9 X. C. Jiang, Q. H. Xiong, S. Nam, F. Qian, Y. Li and C. M. Lieber, *Nano Lett.*, 2007, **7**, 3214.
10 T. Chen, G. Z. Xing, Z. Zhang, H. Y. Chen and T. Wu, *Nanotechnology*, 2008, **19**, 435711.
11 G. P. Li, T. Chen, B. Yan, Y. Ma, Z. Zhang, T. Yu, Z. X. Shen, H. Y. Chen and T. Wu, *Appl. Phys. Lett.*, 2008, **92**, 173104.
12 X. W. Lou, L. A. Archer and Z. C. Yang, *Adv. Mater.*, 2008, **20**, 3987.
13 M. H. Huang, S. Mao, H. Feick, H. Q. Yan, Y. Y. Wu, H. Kind, E. Weber, R. Russo and P. D. Yang, *Science*, 2001, **292**, 1897.
14 X. D. Bai, E. G. Wang, P. X. Gao and Z. L. Wang, *Nano Lett.*, 2003, **3**, 1147.
15 M. Law, L. E. Greene, J. C. Johnson, R. Saykally and P. D. Yang, *Nat. Mater.*, 2005, **4**, 455.
16 A. Tsukazaki, A. Ohtomo, T. Onuma, M. Ohtani, T. Makino, M. Sumiya, K. Ohtani, S. F. Chichibu, S. Fuke, Y. Segawa, H. Ohno, H. Koinuma and M. Kawasaki, *Nat. Mater.*, 2005, **4**, 42.
17 Z. L. Wang and J. H. Song, *Science*, 2006, **312**, 242.
18 Z. P. Wei, Y. M. Lu, D. Z. Shen, Z. Z. Zhang, B. Yao, B. H. Li, J. Y. Zhang, D. X. Zhao, X. W. Fan and Z. K. Tang, *Appl. Phys. Lett.*, 2007, **90**, 042113.
19 J. J. Cole, X. Wang, R. J. Knuesel and H. O. Jacobs, *Nano Lett.*, 2008, **8**, 1477.
20 A. Ohtomo, M. Kawasaki, T. Koida, K. Masubuchi, H. Koinuma, Y. Sakurai, Y. Yoshida, T. Yasuda and Y. Segawa, *Appl. Phys. Lett.*, 1998, **72**, 2466.
21 Y. J. Zeng, Z. Z. Ye, F. Liu, D. Y. Li, Y. F. Lu, W. Jaeger, H. P. He, L. P. Zhu, J. Y. Huang and B. H. Zhao, *Cryst. Growth Des.*, 2009, **9**, 263.
22 Y. W. Heo, D. P. Norton, L. C. Tien, Y. Kwon, B. S. Kang, F. Ren, S. J. Pearton and J. R. LaRoche, *Mater. Sci. Eng. R*, 2004, **47**, 1.

23 H. B. Lu, L. Liao, H. Li, D. F. Wang, Y. Tian, J. C. Li, Q. Fu, B. P. Zhu and Y. Wu, *Eur. J. Inorg. Chem.*, 2008, 2727.
24 P. Shimpi, P. X. Gao, D. G. Goberman and Y. Ding, *Nanotechnology*, 2009, **20**, 125608.
25 N. O. V. Plank, H. J. Snaith, C. Ducati, J. S. Bendall, L. Schmidt-Mende and M. E. Welland, *Nanotechnology*, 2008, **19**, 465603.
26 T. J. Kuo, C. N. Lin, C. L. Kuo and M. H. Huang, *Chem. Mater.*, 2007, **19**, 5143.
27 Z. W. Pan, Z. R. Dai and Z. L. Wang, *Science*, 2001, **291**, 1947.
28 Z. Zhang, J. Gao, L. M. Wong, J. G. Tao, L. Liao, Z. Zheng, G. Z. Xing, H. Y. Peng, T. Yu, Z. X. Shen, C. H. A. Huan, S. J. Wang and T. Wu, *Nanotechnology*, 2009, **20**, 135605.
29 D. L. Guo, X. A. Huang, G. Z. Xing, Z. Zhang, G. P. Li, M. He, H. Zhang, H. Y. Chen and T. Wu, *Phys. Rev. B*, 2011, **83**, 045403.
30 *National Institute of Standards and Technology (NIST) 2007 X-ray photoelectron spectroscopy database*, US Department of Commerce, USA.
31 Y. Yang, R. Scholz, A. Berger, D. S. Kim, M. Knez, D. Hesse, U. Gosele and M. Zacharias, *Small*, 2008, **4**, 2112.
32 Y. H. Gao and Y. Bando, *Nature*, 2002, **415**, 599.
33 S. A. Maier, P. G. Kik, H. A. Atwater, S. Meltzer, E. Harel, B. E. Koel and A. A. G. Requicha, *Nat. Mater.*, 2003, **2**, 229.
34 G. A. DeVries, M. Brunnbauer, Y. Hu, A. M. Jackson, B. Long, B. T. Neltner, O. Uzun, B. H. Wunsch and F. Stellacci, *Science*, 2007, **315**, 358.
35 J. Q. Hu, Y. Bando and D. Golberg, *J. Mater. Chem.*, 2009, **19**, 330.
36 Y. Qin, S. M. Lee, A. Pan, U. Gosele and M. Knez, *Nano Lett.*, 2008, **8**, 114.
37 H. J. Fan, M. Knez, R. Scholz, K. Nielsch, E. Pippel, D. Hesse, M. Zacharias and U. Gosele, *Nat. Mater.*, 2006, **5**, 627.
38 J. Goldberger, R. R. He, Y. F. Zhang, S. W. Lee, H. Q. Yan, H. J. Choi and P. D. Yang, *Nature*, 2003, **422**, 599.
39 H. J. Fan, U. Gosele and M. Zacharias, *Small*, 2007, **3**, 1660.
40 M. Menon and J. W. Bullard, *J. Mater. Chem.*, 1999, **9**, 949.
41 Y. B. Li, Y. Bando, D. Golberg and Z. W. Liu, *Appl. Phys. Lett.*, 2003, **83**, 999.
42 K. K. Zhu, J. C. Hu, C. Kubel and R. Richards, *Angew. Chem. Int. Ed.*, 2006, **45**, 7277.
43 H. B. Lu, L. Liao, H. Li, Y. Tian, J. C. Li, D. F. Wang and B. P. Zhu, *J. Phys. Chem. C*, 2007, **111**, 10273.
44 A. B. Djurisic and Y. H. Leung, *Small*, 2006, **2**, 944.
45 J. H. Li, D. X. Zhao, X. Q. Meng, Z. Z. Zhang, J. Y. Zhang, D. Z. Shen, Y. M. Lu and X. W. Fan, *J. Phys. Chem. B*, 2006, **110**, 14685.
46 J. P. Richters, T. Voss, D. S. Kim, R. Scholz and M. Zacharias, *Nanotechnology*, 2008, **19**, 305202.
47 C. Y. Chen, C. A. Lin, M. J. Chen, G. R. Lin and J. H. He, *Nanotechnology*, 2009, **20**, 185605.
48 Q. Zhao, X. Y. Xu, X. F. Song, X. Z. Zhang, D. P. Yu, C. P. Li and L. Guo, *Appl. Phys. Lett.*, 2006, **88**, 033102.
49 H. Y. Lin, C. L. Cheng, Y. Y. Chou, L. L. Huang, Y. F. Chen and K. T. Tsen, *Opt. Express*, 2006, **14**, 2372.
50 X. Wang, X. G. Kong, Y. Yu and H. Zhang, *J. Phys. Chem. C*, 2007, **111**, 3836.
51 K. Okamoto, I. Niki, A. Shvartser, Y. Narukawa, T. Mukai and A. Scherer, *Nat. Mater.*, 2004, **3**, 601.
52 C. W. Cheng, E. J. Sie, B. Liu, C. H. A. Huan, T. C. Sum, H. D. Sun and H. J. Fan, *Appl. Phys. Lett.*, 2010, **96**, 071107.
53 X. J. Wang, G. P. Li, T. Chen, M. X. Yang, Z. Zhang, T. Wu and H. Y. Chen, *Nano Lett.*, 2008, **8**, 2643.
54 H.-J. Tiller, U. Demme, D. Lenke, P. Bühner and K. Meyer, *Cryst. Res. Technol.*, 1975, **10**, K103.
55 C. Benvenuti, P. Chiggiato, P. C. Pinto, A. E. Santana, T. Hedley, A. Mongelluzzo, V. Ruzinov and I. Wevers, *Vacuum*, 2001, **60**, 57.
56 C. W. Lai, J. An and H. C. Ong, *Appl. Phys. Lett.*, 2005, **86**, 251105.
57 O. Kulakovich, N. Strekal, A. Yaroshevich, S. Maskevich, S. Gaponenko, I. Nabiev, U. Woggon and M. Artemyev, *Nano Lett.*, 2002, **2**, 1449.
58 S. W. Hwang, D. H. Shin, C. O. Kim, S. H. Hong, M. C. Kim, J. Kim, K. Y. Lim, S. Kim, S. H. Choi, K. J. Ahn, G. Kim, S. H. Sim and B. H. Hong, *Phys. Rev. Lett.*, 2010, **105**, 127403.